HCCI와 SACI 조건하에서 희박 이소옥탄/공기 혼합물의 점화특성에 관한 직접수치모사 연구

유춘상*

A DNS study of ignition characteristics of a lean iso-octane/air mixture under HCCI and SACI conditions

Chun Sang Yoo*

ABSTRACT

The effect of thermal stratification, spark-ignition, and turbulence on the ignition of a lean homogeneous *iso*-octane/air mixture at constant volume and high pressure is investigated by direct numerical simulations (DNS) with a new 99-species reduced kinetic mechanism developed for very lean mixtures from the detailed mechanism (Mehl et al., 4th European Combustion Meeting, Vienna, Austria, 2009). Two-dimensional DNS are performed in a fixed volume with two-dimensional isotropic velocity spectrums, temperature fluctuations, and ignition source superimposed on the initial scalar fields. The influence of variations in the initial temperature field imposed by changing the variance of temperature, the ignition-timing by changing the time at which ignition source is superimposed, and the turbulence intensity and length scale on ignition of a lean *iso*-octane/air mixture is elucidated. The mean heat release rate increases more slowly and ignition delay decreases with increasing thermal stratification under homogeneous charge compression-ignition (HCCI) condition since the present mean temperature lies far outside of the negative temperature coefficient (NTC) regime. The spark-ignition induces relatively short ignition delay under spark-assisted compression ignition (SACI) condition while slightly spreading out the mean heat release rate. For SACI combustion, high turbulence intensity decreases the ignition delay more by increasing turbulent flame area. Displacement speed and Damköhler number analyses reveal that the high degree of thermal stratification induces deflagration at the reaction fronts, and hence, the mean heat release rate is smoother subsequent to thermal runaway occurring at the highest temperature regions in the domain. For SACI combustion, the heat release occurs solely by deflagration prior to the occurrence of the maximum heat release and subsequently by the mixed mode of deflagration and spontaneous ignition. These results suggest that the thermal stratification is more effective for smooth operation of HCCI engines and the spark-ignition can precisely control the ignition timing for SACI combustion.

Key Words : DNS, HCCI, SACI, iso-octane/air reduced mechanism, thermal stratification

* 소속: 울산과학기술대학교
† E-mail : csyoo@unist.ac.kr
Tel : (052)217-2322 Fax : (052)217-2309

1. Introduction

Homogeneous charge compression ignition

(HCCI) engines have been developed as an alternative to the conventional internal combustion engines because they are able to achieve high-fuel efficiency and meet contingent environmental regulations. It is attributed to their operating characteristics that HCCI combustion takes place under lean, diluted, high-pressure and low-temperature conditions, and hence, it can provide high diesel-like efficiency with very low NO_x and soot emissions [1-3]. HCCI combustion, however, occurs primarily through volumetric auto-ignition, and hence, it is still challenging to control ignition timing and alleviate high pressure rise rate which may lead to engine knock in high-load conditions.

From extensive experimental and numerical studies by the engine research community, thermal stratification was proposed as a remedy to spread out high pressure rise rate or heat release rate under high-load conditions [1, 4-6]. Mixture inhomogeneities, however, were proposed to enhance and stabilize HCCI combustion under low-load conditions [1, 7-9]. In addition to these stratification of mixture conditions, spark-assisted compression ignition (SACI) has emerged as an additive method to stratification because spark ignition in SACI combustion generates deflagrations before volumetric auto-ignition occurs, which is nearly identical to that of high thermal stratification. Therefore, it can control the ignition timing and spread out the pressure rise rate under both low and high load conditions [10-12].

Experiments, however, can provide only limited information such as overall pressure rise, pollutant emissions, and chemiluminescence of select species. As such, detailed understanding of chemical reactions occurring in an HCCI engine is still elusive. However, ignition characteristics of lean fuel/air mixtures under HCCI conditions were able to be elucidated by direct numerical simulations (DNS) with detailed and reduced chemical kinetic mechanisms [13-17]. From two-dimensional DNS of ignition of lean hydrogen/air mixtures with temperature inhomogeneities [13-15], it was found that, for mixtures with sufficiently large temperature fluctuations, deflagrations first occur rather than volumetric auto-ignition, and consequently, the heat release rate is spread out as the deflagrations propagate through the mixture. It was also found that mixture inhomogeneities together with temperature fluctuations further spread out heat release rate compared to temperature fluctuations only [17]. Recently, DNS of ignition of a lean n-heptane/air mixture with different mean and root-mean-square (RMS) of temperature revealed that ignition characteristics can significantly be changed with different initial mean temperatures [17]; i.e., temperature fluctuation retards overall HCCI combustion when the mean initial temperature lies within the negative-temperature coefficient (NTC) regime. On the contrary, HCCI combustion is enhanced when the mean initial temperature lies sufficiently outside of the NTC regime. For both cases, however, the larger temperature RMS is, the more heat release rate is spread out.

The objective of the present DNS study is to elucidate the combustion characteristics of hydrocarbon fuel/air mixture under both HCCI and SACI conditions by varying the degree of temperature and turbulence fluctuations, and spark-ignition timing. In this study, *iso*-octane is adopted as a surrogate fuel for gasoline.

2. *iso*-Octane/air reduced mechanism

From the detailed *iso*-octane/air kinetic mechanism of Mehl et al. [18], a skeletal mechanism with 266 species and 1294 reactions was obtained, using the reduction strategy combining directed relation graph (DRG) based methods and short time scale analysis [16, 19, 20]. The DRG-aided sensitivity analysis (DRGASA) method, then, was applied to further reduce the skeletal mechanism. Auto-ignition delay and extinction residence time in perfectly stirred reactors (PSR) were targeted in the sensitivity analysis. By specifying a worst case error tolerance of 30 %, a skeletal mechanism with 143 species and 643 reactions was developed. Linearized quasi-steady state approximation (LQSSA) [21]} was further applied to the 143 species skeletal mechanism to reduce the number of transported species. Using a criterion based on

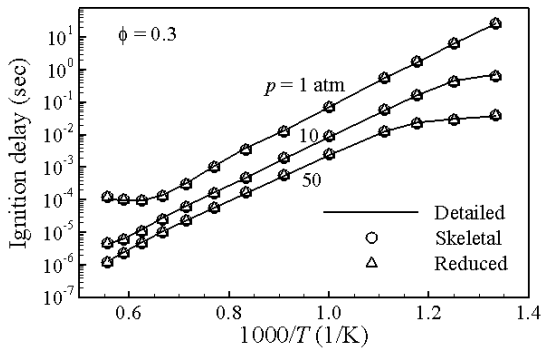

Fig. 1 Comparison of the 143-species skeletal and the 99-species reduced mechanism with the detailed mechanism for iso-octane/air mixtures at different pressures for ϕ = 0.3.

computational singular perturbation (CSP) [22], 44 species were identified as globally valid QSS species, while the associated reactions were analytically solved. A 99 species reduced mechanism was obtained. As the last step, the method of dynamic stiffness removal [16, 19] was employed to eliminate short chemical timescales shorter than 10 ns.

The skeletal and reduced mechanisms were validated through auto-ignition delay and extinction residence time over a wide parameter range of pressure from 1 to 50 atm, equivalence ratio 0.3 - 2.0, and initial temperature 750 - 1800 K. Figure 1 shows the comparison of ignition delays at an equivalence ratio of 0.3 under different constant pressure. It is readily observed that both the skeletal and reduced mechanisms can well reproduce the results of the detailed mechanism. Finally, the laminar flame speeds calculated with the reduced mechanism and those from experimental measurements were compared (not shown here). The results with the reduced mechanism match fairly well those of the experiments.

3. Numerical method and initial conditions

The compressible Navier-Stokes, species continuity, and total energy equations were solved using the Sandia DNS code, S3D [23, 24]. Details of the numerical schemes and libraries used in the present study can be found in [16]. Periodic boundary conditions were imposed in all directions such that ignition of an *iso*-octane/air mixture occurs at constant volume.

The initial uniform equivalence ratio, ϕ, and pressure, p_0, are 0.3 and 20 atm, respectively. Note that the initial pressure and fuel-air ratio is representative of the top dead center (TDC) end-gas conditions in air-diluted HCCI or SACI combustion [25]. Several parametric studies were performed to figure out the effects of varying the fluctuation of temperature for HCCI combustion, the timing of spark-ignition for SACI combustion, and the turbulence for both HCCI and SACI combustion. A total of eleven different DNS cases were performed with different temperature fluctuation RMS, T', spark-ignition timing, τ_s, most energetic turbulent length scale, l_e, and turbulence velocity fluctuation, u'. Turbulence time-scale is defined by $\tau_t = l_e/u'$. For all simulations, mean temperature T_0 = 1035 K and homogeneous ignition delay τ_{ig}^0 = 2.5 ms. Henceforth, τ_{ig} represents the time at which the maximum mean heat release rate occurs, and the superscript 0 corresponds to the zero-dimensional simulation at constant volume. The initial turbulent flow field is prescribed by an isotropic kinetic energy spectrum function as in [13-16]. The initial temperature field is also generated by a temperature spectrum, similar to the kinetic energy spectrum. Note that the two random fields are uncorrelated. Details of the physical parameters for the cases are presented in Table 1.

The computational domain is a two-dimensional square box with each size of the domain, L, of 3.2 mm, discretized with 640 grid points for all cases. The corresponding grid resolution is 5.0 μm. This fine grid resolution is needed to resolve the ignition structure at high pressure. The most energetic length scale of the temperature fluctuation, l_{Te}, is 1.25 mm for all cases.

Typical profiles of initial temperature for HCCI and SACI combustion are shown in Fig. 2. Spark ignition in SACI combustion can be achieved by superimposing high temperature

Table 1 : Physical parameters of the DNS cases

Case	Type	T_0 (K)	T' (K)	l_e (mm)	u' (m/s)	τ_t (ms)	τ_{ig}^0 (ms)	τ_s (ms)
1	HCCI	1035	15	1.25	0.5	2.5	2.5	-
2	HCCI	1035	30	1.25	0.5	2.5	2.5	-
3	HCCI	1035	60	1.25	0.5	2.5	2.5	-
4	SACI	1035	15	1.25	0.5	2.5	2.5	0.0
5	SACI	1035	15	1.25	0.5	2.5	2.5	0.5
6	SACI	1035	15	1.25	0.5	2.5	2.5	1.0
7	SACI	1035	15	1.25	0.5	2.5	2.5	1.5
8	HCCI	1035	15	1.25	2.5	0.5	2.5	-
9	HCCI	1035	15	0.25	0.5	0.5	2.5	-
10	SACI	1035	15	1.25	2.5	0.5	2.5	0.0
11	SACI	1035	15	0.25	0.5	0.5	2.5	0.0

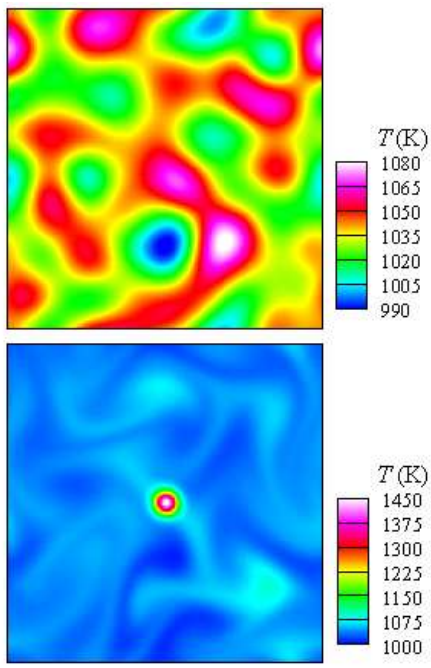

Fig. 2 Initial temperature fields for Cases 1 and 6

source on temperature field at the center of the domain. High temperature source is modeled by a Gaussian profile;

$$T(x,y) = T_m \exp\left[-\frac{(x-x_c)^2+(y-y_c)^2}{2\sigma^2}\right]$$

where x_c and y_c are the centers of x- and y-directions of the domain, respectively and σ was specified as $0.25L$. T_m was specified as 400 K to ignite the mixture in relatively short time (< 0.05 ms) without producing any significant spurious acoustic waves. For SACI combustion (Cases 4-7, 10, and 11), the ignition source was added on top of the temperature field of Case 1 at $t = \tau_s$ and further simulation was performed.

4. Results - effect of temperature fluctuations

As in the previous DNS studies [13-16], the effect of temperature fluctuations on the combustion characteristics of the *iso*-octane/air mixture is elucidated. For this purpose, three different degrees of temperature fluctuation are chosen; i.e., T' = 15, 30, and 60 K for Cases 1-3, respectively. Note that under the present initial temperature and pressure condition, there is no two-stage ignition in *iso*-octane oxidation and hence, homogeneous ignition delay does not exhibit NTC regime as shown in Fig. 1.

Figure 3 shows the temporal evolution of mean pressure, $\bar{p}$, and heat release rate, $\bar{\dot{q}}$, for different levels of temperature fluctuations (Cases 1-3). For comparison, the temporal evolution of the corresponding 0-D homogeneous ignition is also shown in the

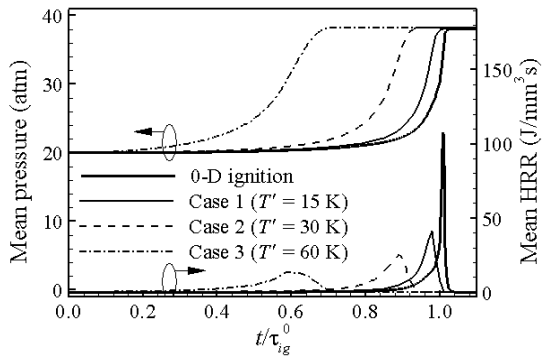

Fig. 3 Temporal evolution of mean pressure and heat release rate for Cases 1-3.

figure. It is readily observed that $\bar{p}$ increases more slowly and $\bar{\dot{q}}$ becomes smoother with increasing T'. In addition, τ_{ig} and the peak $\bar{\dot{q}}$ also decrease with increasing T'. These results are qualitatively similar to those of ignition of a lean hydrogen/air mixture [14, 15] and of a lean *n*-heptane/air mixture with high initial mean temperature [16]. As discussed in [14-16], HCCI combustion with small T' occurs primarily through spontaneous ignition and hence, the combustion characteristics are similar to those of homogeneous auto-ignition. However, for large T', high $\dot{q}$ occurs primarily in thin sheets, although relatively low $\dot{q}$ also occurs over a much broader area. Therefore, this suggests that the combustion mode is sensitive to the level of T'; i.e., the spontaneous ignition mode seems to be predominant for small T' while the mixed mode of deflagration and spontaneous ignition seems to occur for large T'.

To examine the overall structure of the heat release rate field, isocontours of heat release rate, $\dot{q}$, for Cases 1-3 approximately at each τ_{ig} are shown in Fig. 4. $\dot{q}$ is normalized by the corresponding maximum heat release rate during the 0-D homogeneous ignition, $\dot{q}_m^0$ = 107 J/mm^{3}s. It is readily observed from the figure that $\dot{q}$ occurs nearly simultaneously over a wide area of the domain as spontaneous ignition for small T' (Case 1), although relatively high $\dot{q}$ also occurs in thin sheets. For large T' (Case 3), however, high $\dot{q}$ occurs primarily in thin sheets. Note that for Case 1, the combustion process completely ends in $0.02\tau_{ig}^0$ past τ_{ig} while it continues nearly $0.12\tau_{ig}^0$ after τ_{ig} for Case 3. These results suggest that the spontaneous ignition mode seems to be predominant for small T' while the deflagration seems to primarily occur for large T'.

To figure out the combustion modes (spontaneous ignition versus deflagration) in HCCI combustion, the density-weighted displacement speed, S_d^*, is evaluated, which has been used to distinguish between deflagrations and spontaneous ignition fronts in HCCI combustion [14-16]. S_d^* is defined by [26, 27]:

$$S_d^* = \frac{1}{\rho_u |\nabla Y_k|}\left(\dot{\omega}_k - \frac{\partial}{\partial x_j}(\rho Y_k V_{j,k})\right)$$

where Y_k, $V_{j,k}$, and $\dot{\omega}_k$ denote species mass fraction, species diffusion velocity in the *j*-direction and net production rate of species *k*, respectively, and ρ_u is the density of the unburnt mixture. ρ_u is calculated from the local enthalpy and fresh mixture condition assuming pressure and enthalpy remain constant across the front [14-16]. In the present study, the isocontour of $Y_c = Y_{CO2} + Y_{CO} = 0.045$ is chosen to evaluate the displacement speed. This particular isocontour coincides approximately with the location of maximum $\dot{q}$.

Figure 5 shows the temporal evolution of the mean front speed, $\overline{S_d^*}$, normalized by the corresponding laminar flame speed, S_L, for Cases 1-3. As in the previous study [16], S_L was estimated from transient one-dimensional reactive simulation. The simulation was initialized with a high-temperature ignition source such that a combustion wave emanates from the source, propagating into the reactive mixture ahead of it. From the simulation, S_L is found to be approximately 0.45 m/s. It is readily observed from Fig. 5 that the mean front speeds exhibit a characteristic 'U' shape qualitatively similar to those found in [14-16]. The occurrence of the 'U'-shaped mean front speed is attributed to the initial thermal

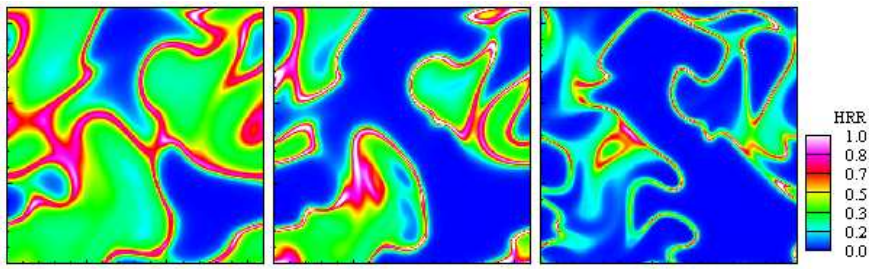

Fig. 4 Isocontours of normalized heat release rate for Cases 1-3 (from left to right) at t/τ_{ig}^0 = 0.97, 0.89, and 0.58, respectively.

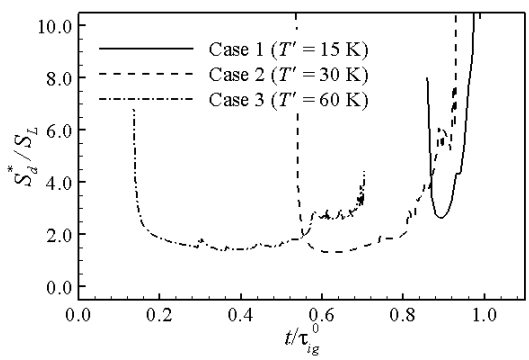

Fig. 5 Temporal evolution of mean front speed for Cases 1-3.

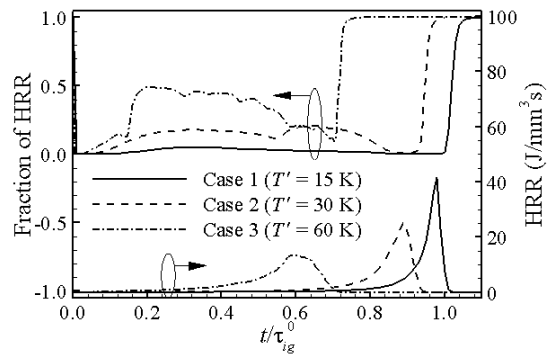

Fig. 6 Temporal evolution of fraction of heat release rate and mean heat release rate for Cases 1-3.

runaway in the nascent ignition kernel during the early phase of combustion and the burnout of remaining charge due to compression heating during the last phase of combustion [16, 28]. Comparison between Figs. 4 and 5 verifies that deflagration waves develop past initial thermal runaway for the cases with large T'.

To quantitatively measure the occurrence of deflagration and spontaneous ignition modes in the combustion process, the temporal evolution of the fraction of heat release rate occurring by the deflagration mode for Cases 1-3 is shown in Fig. 6. To distinguish between the two modes of propagation, the Damköhler number, Da, defined by [27, 29, 30], is adopted:

$$Da = \frac{\dot{\omega}_k}{\left| -\nabla \cdot (\rho Y_k \boldsymbol{V_k}) \right|}$$

where Y_c is used for the Damköhler number analysis. From one-dimensional laminar simulation, it is found that Da in the diffusive limit is approximately 2.5, where the diffusive without auto-ignition, where the diffusion balances reaction. Note that the departure of Da in the diffusive limit from unity is because, although the combustion wave propagates under the diffusive limit, the upstream mixture is highly reactive and hence, the reaction term is somewhat larger than the diffusion term [16]. In the present study, the delineation between the two propagation modes is defined by Da less than 2.5 (deflagration wave).

Several observations can be made from Fig. 6. First, the fraction of $\dot{q}$ from the deflagration mode increases with increasing T', such that nearly half of $\dot{q}$ occurs in the deflagration mode for Case 3 with large T' during the most combustion process. Second, for small T', the fraction of $\dot{q}$ from the deflagration mode is negligible (Case 1) and vanishes much sooner than the occurrence of the peak $\bar{\dot{q}}$ (Case 2); on the contrary, for

large T' (Case 3), a considerable fraction of $\dot{q}$ still occurs in the deflagration mode at the point when $\overline{\dot{q}}$ peaks. It is noted that, at final stage of the ignition, the fraction of $\dot{q}$ from the deflagration mode becomes unity simply because the corresponding reaction rate vanishes, and thus, Da also vanishes. As discussed in the previous studies [14-16], at the final stage of ignition, the remaining unburned charge is heated by compression and consumed as simultaneous ignition, exhibiting large values of S_d^*. Therefore, only a small fraction of combustion occurs in the deflagration mode during the final stages of ignition, verifying that spontaneous auto-ignition occurs for small T'. However, a relatively large fraction of the deflagration mode with large T' indicates the occurrence of mixed modes of deflagration and spontaneous ignition. These results, further, verify that deflagration is attributed to spreading out the heat release rate.

5. Results - effect of spark-ignition timing

In addition to temperature and mixture inhomogeneities, spark-ignition was proposed to control the ignition timing and spread out the pressure rise rate in HCCI combustion. In the present study, therefore, the effect of spark-ignition timing, τ_s, on SACI combustion is studied. The spark ignition is modeled as a high temperature ignition source as described in Section 3. Four simulations were performed with different τ_s (Cases 4-7). See Table 1 for the details of physical parameters for the cases.

The overall combustion characteristics are investigated by examining the temporal evolution of $\overline{p}$ and $\overline{\dot{q}}$ for different τ_s (Cases 4-7) a shown in Fig. 7. The evolution of $\overline{p}$ and $\overline{\dot{q}}$ for Case 1 is also shown as a reference. It is readily observed that τ_{ig} decreases with decreasing τ_s as expected, while the overall shape of mean $\overline{\dot{q}}$ remains qualitatively the same as in Case 1 and the peak $\overline{\dot{q}}$ decreases slightly. It is also found that

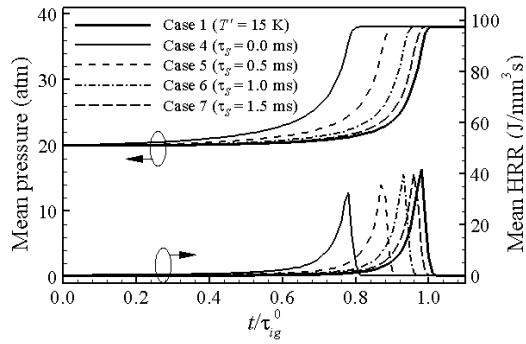

Fig. 6 Temporal evolution of mean pressure and heat release rate for Cases 1 and 4-7.

the pressure increases more smoothly and the heat release rate is more spread out with decreasing τ_s, although the effect of spark-ignition timing is less significant compared to that of T'. Overall, the evolutions of SACI combustion seem qualitatively similar to that of the reference HCCI combustion (Case 1).

To further examine the overall combustion characteristics, isocontours of normalized $\dot{q}$ for Case 4 at different times are shown in Fig. 8. During the early phase of combustion, $\dot{q}$ occurs only in a single corrugated thin sheet as shown in the first two snap shots. Subsequently, the whole remaining mixtures are consumed rapidly past τ_{ig} as shown in the last two snap shots. This result is the opposite to what is expected from Fig. 7, suggesting that combustion initially occurs by deflagration and subsequently by spontaneous ignition of the remaining charge by the compression heating.

To further identify the combustion mode in SACI combustion, the temporal evolution of $\overline{S_d^*}$ and fraction of $\overline{\dot{q}}$ from deflagration is shown in Fig. 9. Although $\overline{S_d^*}$ for fast τ_s (Cases 4--6) are qualitatively identical to that of high T' (Case 3), the whole heat release occurs by deflagration rather than the mixed mode of combustion prior to τ_{ig} as shown in Fig. 9(b). Furthermore, the heat release from the spontaneous ignition covers over 50 % of the total only during the final phase of combustion. In summary, the spark-ignition in

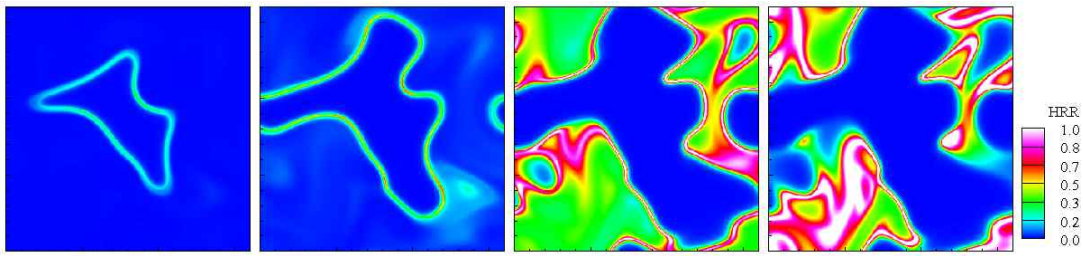

Fig. 8 Isocontours of normalized heat release rate for Case 4. From left to right, t/τ_{ig}^0 = 0.52, 0.68, 0.77 and 0.78, respectively.

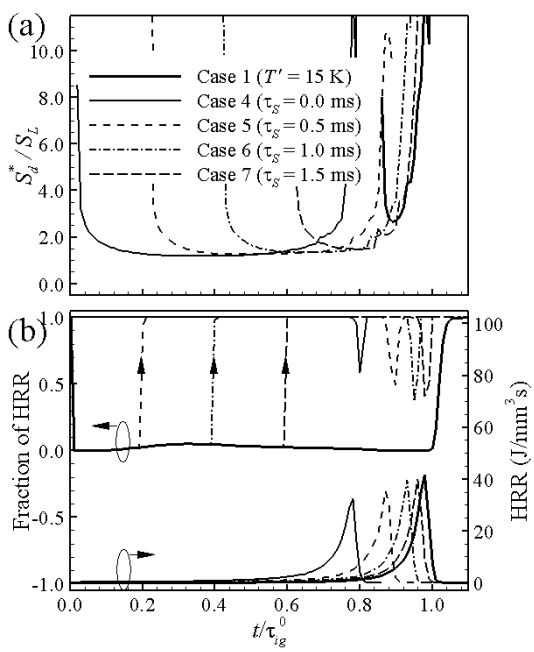

Fig. 9 Temporal evolution of mean pressure and heat release rate for Cases 1 and 4-7.

Cases 4-7 initiates and enhances the overall combustion. The heat release, however, occurs solely by deflagration except for the final phase of combustion with a mixed mode of deflagration and spontaneous ignition.

6. Results - effect of turbulence

In SACI combustion, the early evolution of turbulent flames plays a critical role in determining combustion rate or heat release

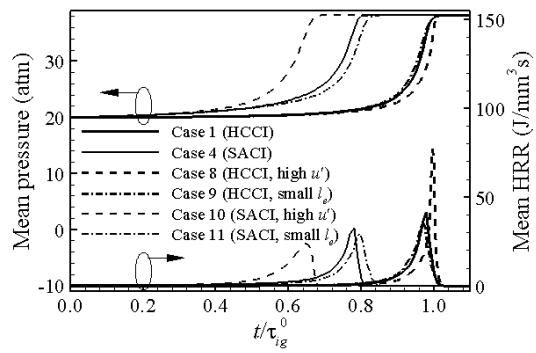

Fig. 10 Temporal evolution of mean pressure and heat release rate for Cases 1, 4, and 8-11.

rate. It is attributed to that by definition, the turbulent burning velocity is proportional to the flame surface area and the laminar flame speed [31]. In this section, therefore, the effect of turbulence on HCCI and SACI combustion is elucidated. Four additional simulations (Cases 8-11) are performed with different turbulence intensity and length scale under both HCCI and SACI conditions. Note that the four cases have the same turbulence time scale which is five times as fast as those in other cases, while having different u' and l_e. Details of the parameters are shown in Table 1.

Figure 10 shows the temporal evolution of mean pressure and heat release rate for the cases. For comparison purpose, Cases 1 and 4 are also shown in the figure. Several points are to be noted from the figure. From the previous DNS study of ignition of an *n*-heptane/air mixture under HCCI condition

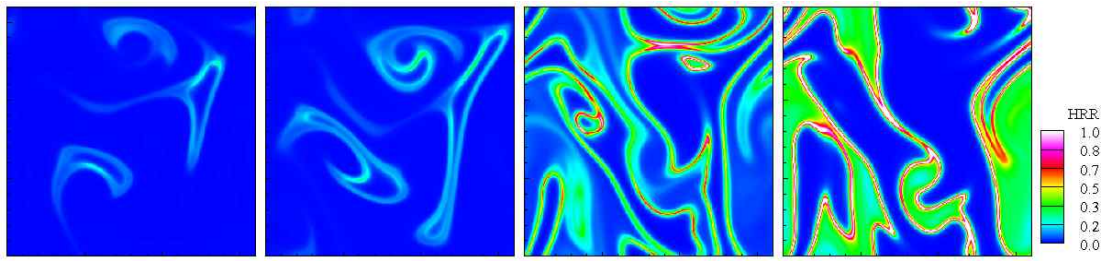

Fig. 11 Isocontours of normalized heat release rate for Case 9. From left to right, t/τ_{ig}^0 = 0.40, 0.48, 0.60, and 0.64, respectively.

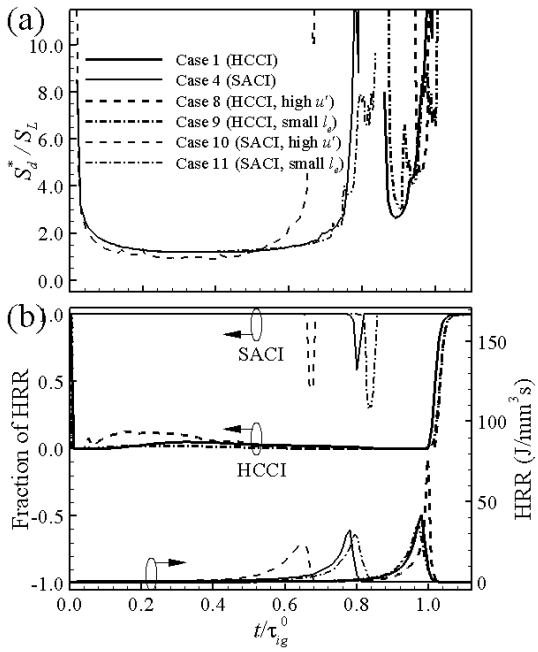

Fig. 12 Temporal evolution of mean pressure and heat release rate for Cases 1 and 1, 4, and 8-11.

[16], it was found that usually, turbulence with a fast τ_t is able to homogenize the mixture such that ignition is more apt to occur by spontaneous ignition. In the present study, however, the ratio between the temperature fluctuation and turbulence length scales is also found to play an important role in homogenizing the mixture. Although τ_t in Cases 8 and 9 are identical, τ_t in Case 9 has no significant effect in homogenizing the mixture, while τ_t in Case 8 effectively homogenizes the mixture, rendering the overall combustion similar to 0-D homogeneous ignition. This is because l_e in Case 9 is much smaller than l_{Te} and as such, fast mixing by a fast τ_t occurs only in a length scale smaller than l_{Te}., suggesting no effective homogenization of temperature. However, l_e. in Case 8 identical to l_{Te} together with high u' can effectively homogenize the mixture, resulting in the similar combustion characteristics to the 0-D homogeneous ignition.

For SACI combustion (Cases 4, 10, and 11), high u' significantly enhances the overall combustion for Case 10, while small l_e has no significant effect in Case 11. As mentioned above, high u' increases turbulent burning velocity by significantly increasing flame area, resulting in the enhancement of overall combustion. Figure 11, showing the isocontour of heat release rate for Case 9 at different times, verifies the mechanism of increase of flame area by turbulence with high u' compared to Fig. 8. While the combustion characteristics in Case 4 exhibits a single flame evolution during the early phase of combustion, turbulence with high u' in Case 9 divides the nascent flame originated from spark-ignition into several flames, resulting in significant increase of flame area. However, small l_e (Case 11) does not effectively increase the flame area such that the overall combustion is retarded compared to that of Case 4. Note that the effect of u' on the ignition characteristics under SACI conditions highly depends on the size of the domain and the relative size of turbulence length scale, which is an ongoing research topic.

Finally, the temporal evolution of $\overline{S_d^*}$ and

fraction of heat release rate from deflagration mode is shown in Fig. 12 to further identify the combustion mode. As in other HCCI and SACI cases with small T' (Cases 1 and 4), the whole heat release occurs nearly by spontaneous ignition for HCCI combustion and by deflagration for SACI combustion, respectively.

7. Conclusions

The effects of thermal stratification, spark-ignition timing, and turbulence intensity and length scale on auto-ignition of a lean homogeneous *iso*-octane/air mixture at constant volume and high pressure are investigated by direct numerical simulations with a new 99-species reduced *iso*-octane/air kinetic mechanism. In the first parametric study, three cases of HCCI combustion were studied with different degrees of temperature fluctuations. The displacement speed and Damköhler number analyses verify that, in general, larger T' induces greater temporal spreading of the mean heat release rate because the deflagration mode is predominant at the reaction fronts for large T'. However, spontaneous ignition prevails for small T', and hence, simultaneous auto-ignition occurs throughout the whole domain, resulting in an excessive rate of pressure rise.

In the second parametric study, the effect of different spark-ignition timing on SACI combustion was investigated. In general, ignition delay decreases with decreasing τ_s, while the spread of heat release rate is minimal. The displacement speed and Damköhler number analyses verify that the heat release occurs only by deflagration prior to the occurrence of the maximum heat release rate and subsequently, occurs by the mixed combustion mode of deflagration and spontaneous ignition by compression heating of the remaining charge.

Finally, in the third parametric study the effect of turbulence intensity and length scale was elucidated. For HCCI combustion, usually a fast turbulence timescale is able to homogenize the mixture such that ignition is more apt to occur by spontaneous ignition [16]. However, it is found that small l_e compared to l_{Te} has no significant mixing effect in spite of a fast τ_t by high u'. For SACI combustion, turbulence with high u' significantly enhances the overall combustion by inducing many deflagration waves, leading to the mixed mode of combustion at the last phase of combustion.

These results imply that the thermal stratification is needed for smooth operation of pure HCCI engines and the spark-ignition can effectively be used to control the ignition timing under SACI condition.

Acknowledgement

This paper was submitted to 34th international symposium on combustion. This work was supported by Basic Science Research Program through the National Research Foundation of Korea (NRF) funded by the Ministry of Education, Science and Technology (Grant No. 2011-0008201).

References

[1] J. E. Dec, Proc. Combust. Inst. 32 (2009) 2727-2742.
[2] M. Yao, Z. Zheng, H. Liu, Prog. Energy Combust. Sci. 35 (2009) 398-437.
[3] X. L□u, D. Han, Z. Huang, Prog. Energy Combust. Sci. 37 (2011) 741-783.
[4] A. Hultqvist, M. Christenson, B. Johansson, M. Richter, J. Nygren, J. Hult, M. Alden, SAE paper (2002) 2002-01-0424.
[5] A. Babajimopoulos, G. A. Lavoie, D. N. Assanis, SAE paper (2003) 2003-01-3220.
[6] M. Sjöberg, J. E.Dec, SAE Trans. paper 115 (2006) 318-334.
[7] M. Richter, J. Engstr□om, A. Franke, M. Alden, A. Hultqvist, B. Johansson, SAE Trans. paper (2000) 2000-01-2868.
[8] P. W. Aroonsrosopon, P. Werner, J. O. Waldman, SAE Tran. paper 113 (2004) 2004-01-1756.
[9] W. Hwang, J. E. Dec, M. Sjöberg, SAE Trans. paper 116 (2007) 2007-01-4130.
[10] L. Koopmans, I. Denbratt, SAE paper (2001) 2001-01-3610.
[11] A. Fuhhapter, W. F. Piock, G. K. Fraidl, SAE paper (2003) 2003-01-0754.
[12] H. Persson, A. Hultqvist, B. Johanass,

A. Remon, SAE paper (2007) 2007-01-0212.
[13] R. Sankaran, H. G. Im, E. R. Hawkes, J. H. Chen, Proc. Combust. Inst. 30 (2005) 875-882.
[14] J. H. Chen, E. R. Hawkes, R. Sankaran, S. D. Mason, H. G. Im, Combust. Flame 145 (2006) 128-144.
[15] E. R. Hawkes, R. Sankaran, P. Pebay, J. H. Chen, Combust. Flame 145 (2006) 145-159.
[16] C. S. Yoo, T. Lu, J. H. Chen, C. K. Law, Combust. Flame 158 (2011) 1727-1741
[17] G. Bansal, H. G. Im, Combust. Flame 158 (2011) 2105-2112.
[18] M. Mehl, H. J. Curran, W. J. Pitz, C. K. Westbrook, Chemical kinetic modeling of component mixtures relevant to gasoline, in: 4th European Combustion Meeting, Vienna, Austria, 2009.
[19] T. Lu, C. K. Law, C. S. Yoo, J. H. Chen, Combust. Flame 156 (2009) 1542-1551.
[20] T. Lu, C. K. Law, Prog. Energy Combust. Sci. 35 (2009) 192-215.
[21] T. Lu, C. K. Law, J. Phys. Chem. A 110 (2006) 13202-13208.
[22] T. Lu, C. K. Law, Combust. Flame 154 (2008) 761-774.
[23] J. H. Chen et al., Comput. Sci. Disc. 2 (2009) 015001.
[24] J. H. Chen, Proc. Combust. Inst. 33 (2011) 99-123.
[25] J. B. Martz, H. Kwak, H. G. Im, Lavoie, D. Assanis, Proc. Combust. Inst. 33 (2011) 3001-3006.
[26] C. S. Yoo, H. G. Im, Proc. Combust. Inst. 30 (2005) 349-356.
[27] C. S. Yoo, R. Sankaran, J. H. Chen, J. Fluid Mech. 640 (2009) 453-481.
[28] C. S. Yoo, J. H. Chen, J. H. Frank, Combust. Flame 156 (2009) 140-151.
[29] T. Echekki, J. H. Chen, Combust. Flame 134 (2003) 169-191.
[30] C. S. Yoo, E. S. Richardson, R. Sankaran, J. H. Chen, Proc. Combust. Inst. 33 (2011) 1619-1627.
[31] C. K. Law, Combustion physics, Cambridge University Press, 2006.